

Efficient CDF Approximations for Normalizing Flows

Chandramouli Sastry^{1 2 3} Andreas Lehrmann¹ Marcus Brubaker^{1 2 4} Alexander Radovic¹

Abstract

Normalizing flows model a complex target distribution in terms of a bijective transform operating on a simple base distribution. As such, they enable tractable computation of a number of important statistical quantities, particularly likelihoods and samples. Despite these appealing properties, the computation of more complex inference tasks, such as the cumulative distribution function (CDF) over a complex region (e.g., a polytope) remains challenging. Traditional CDF approximations using Monte-Carlo techniques are unbiased but have unbounded variance and low sample efficiency. Instead, we build upon the diffeomorphic properties of normalizing flows and leverage the divergence theorem to estimate the CDF over a closed region in target space in terms of the flux across its *boundary*, as induced by the normalizing flow. We describe both deterministic and stochastic instances of this estimator: while the deterministic variant iteratively improves the estimate by strategically subdividing the boundary, the stochastic variant provides unbiased estimates. Our experiments on popular flow architectures and UCI benchmark datasets show a marked improvement in sample efficiency as compared to traditional estimators.

1. Introduction

Normalizing Flows (Kobyzev et al., 2020; Papamakarios et al., 2021) are a form of generative model which constructs tractable probability distributions through invertible, differentiable transformations, *i.e.*, diffeomorphisms. They admit both efficient and exact density evaluation and sampling and, as valid probability distributions, theoretically support a range of other probabilistic inference tasks. However, some inference tasks remain computationally challenging. Here we consider the task of computing cumulative densi-

¹Borealis AI ²Vector Institute ³Dalhousie University ⁴York University. Correspondence to: Chandramouli Sastry <chandramouli.sastry@gmail.com>.

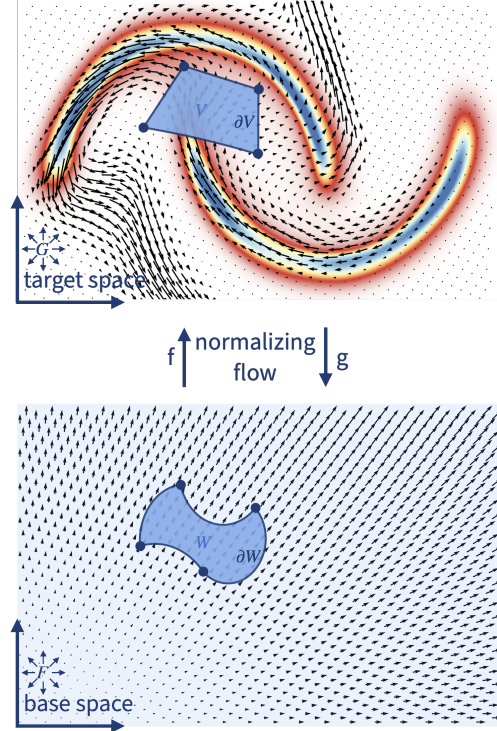


Figure 1. Overview. We propose an efficient estimator to compute the cumulative density P induced by a normalizing flow f over a complex region V . We show that P corresponds to integrating over the boundary $\partial W = g(\partial V)$ in a uniform base space w.r.t. a vector field F with constant divergence 1, which can be expressed as an integration over the boundary ∂V in the target space w.r.t. an equivalent vector field G .

ties over arbitrary closed regions of distributions represented by a normalizing flow. Cumulative densities are a fundamental statistical measure. They answer the question: what is the probability of a sample in this range of values? Example applications are particularly common in the domain of uncertainty estimation (Liu et al., 2019; Mazaheri et al., 2020; Abdar et al., 2021), and the evaluation of risk in financial settings (Richardson et al., 1997; Mehta et al., 2012). Other recent examples include distributional reinforcement learning (Sun et al., 2021), few-shot learning (Ridgeway & Mozer, 2018), and alternative methods for training normalizing flows (Dai & Seljak, 2021).

Despite the importance of cumulative densities, current techniques for computing them with normalizing flows are restricted to traditional Monte-Carlo based estimators which, while unbiased, can have unbounded variance and poor computational efficiency. Further, such approaches fail to exploit the inherent structure of normalizing flows, namely their construction as a diffeomorphic transformation.

In this paper we describe a novel estimator that exploits the unique characteristics of normalizing flows to efficiently estimate the cumulative density in closed regions. To do this we exploit the homeomorphic property of normalizing flow transforms to relate the cumulative density in the target space to volume in the base space. Next we adapt the divergence theorem to show that we only need to consider the boundary of the region in the target space. We analyze the resulting theoretical estimator to identify best-case performance scenarios and use this analysis to motivate an adaptive, approximate estimator. To practically realize this estimator and evaluate its performance, we explore its application to computation of cumulative density over convex regions.

Contributions. The contributions of this paper are as follows. First, we derive a novel formulation of the cumulative density of a normalizing flow by relating it to the volume in a (uniform) base space and the boundary integrals in both base and data space based on the divergence theorem. Second, based on this we describe an unbiased, stochastic estimator for cumulative densities over a closed region. Next, we analyze this estimator to build an adaptive, deterministic approximation for cumulative densities over a closed region by strategically adding points along the boundary of the region. Finally, we describe a comprehensive evaluation protocol to evaluate CDF estimators for normalizing flows as a function of region sizes, architecture families and capacities. The code to reproduce our results, including training popular normalizing flow architectures, approximating cumulative densities with the proposed adaptive boundary estimator and other baseline methods is publicly available.¹

2. Related Work

Our proposed method is principally related to two bodies of existing work: (1) algorithms for efficient estimation of cumulative densities for popular distribution functions; and (2) modifications of popular normalizing flows architectures to allow for more efficient cumulative density estimation.

Classic Algorithms. Computing cumulative densities is not tractable in higher dimensions even for distributions such as the multivariate Gaussian which have closed-form density functions. Consequently, approximations to volume

integrals/cumulative density functions have been an important research problem: for example, (Genz & Bretz, 2009) discuss methods for approximating integrals over multivariate Gaussian and t-distributions. (Botev & l’Ecuyer, 2015) and (Botev, 2017) propose a tilting method for i.i.d. sampling and approximating cumulative densities over convex polytopes in multivariate Gaussian and t-distributions respectively. Approximating integrals over 1D distributions is also challenging for certain distributions; see (Lange, 1999) for a discussion on quadrature methods and chapters 4-6 of (Press et al., 1988) for a discussion on numerical methods for estimating 1D integrals. (Cunningham et al., 2013) extensively study Expectation-Propagation (Minka, 2001) as an approximate integration method for computing cumulative densities over polyhedral or hyperrectangular regions in Gaussian space; if we consider the base space of a normalizing flow to be Gaussian, one could consider – based on our discussion in the methods section – applying this method to the region in Gaussian space corresponding to the region V in the target space; however, it is not easy to ensure that polyhedral regions in target space remain polyhedral in base space without restricting the expressive power of the flow transform.

Normalizing Flows. (Cundy & Ermon, 2020) consider the general problem of estimating integrals and propose an approximate inference procedure that allows explicit control of the bias-variance tradeoff; the method involves first creating partitions of the base uniform space of the normalizing flow and then training a separate variational approximator for each partition: when one partition is used for the entire region, the algorithm reduces to the standard variational approximation resulting in a biased low-variance estimate – however, for an exact estimate, the number of partitions have to be increased and the algorithm reduces to Monte-Carlo sampling. Furthermore, it is not easy to determine the partitioning strategy to arrive at the exact estimate with as few samples as possible. Similar to our problem setting, (Liang et al., 2020) consider the problem of approximating range densities in a tabular database using auto-regressive models: in order to efficiently marginalize over data dimensions, they train the model by randomly masking few data dimensions, which is referred to as variable-skipping. At inference time, they only need to sample the variables whose ranges are specified to form the estimate; even though the training objective is indeed the maximum-likelihood objective, the estimate obtained from the model trained with variable-skipping technique is only an approximate value of the range densities. (Chilinski & Silva, 2020) suggest an alternative to normalizing flows with some similarities, where CDF estimates are available through a simple forward pass. However, this new model family has some limitations in comparison to normalizing flows, most notably sampling from the learned distribution is not supported.

¹ <https://github.com/BorealisAI/nflow-cdf-approximations>

3. Background

Before we describe our approach we provide a brief review of normalizing flows and traditional sampling-based methods of estimating their cumulative densities.

3.1. Normalizing Flows

Normalizing flows transform a random variable \mathbf{Y} with a simple base distribution $p_{\mathbf{Y}}(\mathbf{y})$ into a random variable \mathbf{X} with a complex target distribution $p_{\mathbf{X}}(\mathbf{x})$ using a bijective mapping $f : \mathbb{R}^d \rightarrow \mathbb{R}^d$. Base and target space are connected by the change-of-variables formula

$$p_{\mathbf{X}}(\mathbf{x}) = p_{\mathbf{Y}}(\mathbf{y}) \left| \det \frac{dg}{d\mathbf{x}} \right|, \quad (1)$$

where g is the inverse of f . We set $\mathbf{Y} \sim \mathcal{U}_{[0,1]^d}$, which has the important property $P(\mathbf{y} \in \mathbf{W}) = \text{vol}(\mathbf{W})$ for any compact set $\mathbf{W} \subset [0, 1]^d$, i.e., the cumulative density equals the enclosed volume.² For pre-existing flows f' with non-uniform (e.g., Gaussian) base distribution $p_{\mathbf{Y}'}(\mathbf{y}')$, we can simply set $f := f'(F_{\mathbf{Y}'}^{-1}(\mathbf{y}))$ to align them with the case above. Sampling from a normalizing flow involves first sampling $\mathbf{y} \sim p_{\mathbf{Y}}$ and then applying the flow transform f to obtain $\mathbf{x} = f(\mathbf{y})$.

Objective. Given a compact set of interest $\mathbf{V} \subset \mathbb{R}^d$ in target space, our goal will be the efficient computation of

$$P(\mathbf{x} \in \mathbf{V}) = \int_{\mathbf{V}} p_{\mathbf{X}}(\mathbf{x}) d\mathbf{x}. \quad (2)$$

3.2. Monte-Carlo Estimation

If the volume \mathbf{V} admits a tractable membership function, one could estimate $P(\mathbf{x} \in \mathbf{V})$ from N random samples from the model as the fraction of points falling into \mathbf{V} ; we refer to this method as the *Monte-Carlo (MC) estimate*. Similarly, if the volume \mathbf{V} admits a uniformly distributed random variable $\mathbf{U} \sim \mathcal{U}_{\mathbf{V}}$, one could estimate $P(\mathbf{x} \in \mathbf{V})$ as

$$\int_{\mathbf{V}} p_{\mathbf{X}}(\mathbf{x}) d\mathbf{x} = \int_{\mathbf{V}} p_{\mathbf{U}}(\mathbf{x}) \cdot \frac{p_{\mathbf{X}}(\mathbf{x})}{p_{\mathbf{U}}(\mathbf{x})} d\mathbf{x} = \mathbb{E}_{\mathbf{x} \sim p_{\mathbf{U}}} \left[\frac{p_{\mathbf{X}}(\mathbf{x})}{p_{\mathbf{U}}(\mathbf{x})} \right],$$

which we refer to as the *Importance Sampling (IS) estimate*. While both of the described estimators are unbiased, they have unbounded variances for smaller sample sizes and may require several runs to obtain accurate results (Cunningham et al., 2013).

4. Efficient Estimation of Cumulative Densities

Equipped with these tools, we will now describe our technique to efficiently compute the cumulative density of

Eq.(2). We proceed in three steps: first, we leverage the divergence theorem to relate $P(\mathbf{x} \in \mathbf{V})$ to a flux through the *transformed* boundary $g(\partial\mathbf{V})$ of \mathbf{V} in base space (Section 4.1). Then, we introduce an equivalent flux through the *untransformed* boundary $\partial\mathbf{V}$ of \mathbf{V} to enable direct integration in target space (Section 4.2). Finally, we propose an iterative protocol that enables fine-grained control over the quality of the approximation (Section 4.3).

4.1. Cumulative Density as Boundary Flux

We will first show that computing the cumulative density over \mathbf{V} in target space is equivalent to computing the volume of $\mathbf{W} := g(\mathbf{V})$ in base space.

Lemma 1. Let $\mathbf{V} \subset \mathbb{R}^d$ be compact and $\mathbf{W} := g(\mathbf{V})$. Then $P(\mathbf{x} \in \mathbf{V}) = \text{vol}(\mathbf{W})$.

Proof. Noting that $p(\mathbf{x}) = p(\mathbf{y}) \left| \det \frac{dg}{d\mathbf{x}} \right|$ and $d\mathbf{y} = \left| \det \frac{dg}{d\mathbf{x}} \right| d\mathbf{x}$, we have

$$\begin{aligned} P(\mathbf{x} \in \mathbf{V}) &= \int_{\mathbf{V}} p(\mathbf{x}) d\mathbf{x} = \int_{\mathbf{V}} p(\mathbf{y}) \left| \det \frac{dg}{d\mathbf{x}} \right| d\mathbf{x} \\ &= \int_{\mathbf{W}} p(\mathbf{y}) d\mathbf{y} = \int_{\mathbf{W}} d\mathbf{y} = \text{vol}(\mathbf{W}) \quad \square \end{aligned} \quad (3)$$

We can control the properties of \mathbf{W} through f :

Definition 1 (Diffeomorphism). A differentiable bijection f on \mathbb{R}^d is called a diffeomorphism, if it has a differentiable inverse $g = f^{-1}$.

Importantly, diffeomorphisms map points on the boundary to points on the boundary and points in the interior to points in the interior (Armstrong, 2013), implying $\partial\mathbf{W} = g(\partial\mathbf{V})$ for any diffeomorphic flow f . This includes popular flow architectures like Glow (Kingma & Dhariwal, 2018), MAF (Papamakarios et al., 2017), and FFIORD (Grathwohl et al., 2019) and ensures that \mathbf{W} meets the requirements for the following theorem relating volume integrals to surface integrals.

Theorem 1 (Divergence Theorem). Let $\mathbf{T} \subset \mathbb{R}^d$ be compact with piecewise smooth boundary $\partial\mathbf{T}$. Given a vector field \mathbf{B} , the volume integral of the divergence $\nabla \cdot \mathbf{B}$ over \mathbf{T} and the surface integral of \mathbf{B} over $\partial\mathbf{T}$ are related by

$$\int_{\mathbf{T}} (\nabla \cdot \mathbf{B}) d\mathbf{T} = \int_{\partial\mathbf{T}} \mathbf{B} \cdot \mathbf{n} d(\partial\mathbf{T}), \quad (4)$$

where \mathbf{n} is the outward-facing unit normal.

Proof. (Wade, 2017) \square

Setting $\mathbf{A} := \partial\mathbf{W}$, an application of the divergence theorem using the vector field $\mathbf{F}(\mathbf{x}) = d^{-1}\mathbf{x}$ yields $\text{div}(\mathbf{F}) = 1$ and

²We use \mathcal{U}_S to denote the uniform distribution with support S .

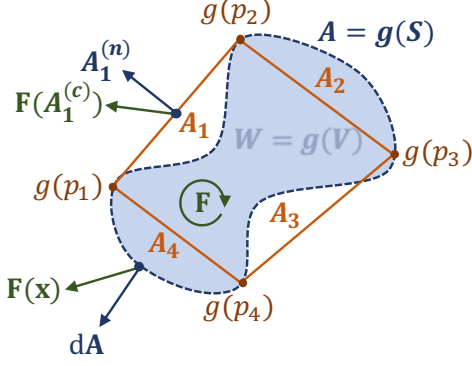


Figure 2. Estimation in Base Space. A piecewise linear boundary \mathbf{S} defined by points $\{p_i\}_i$ in target space has a complex shape \mathbf{A} in base space. The cumulative density enclosed by \mathbf{S} is equivalent to the boundary flux of \mathbf{F} through \mathbf{A} (Eq.(5)). As an approximation, we can instead compute the boundary flux of \mathbf{F} through the piecewise linear boundary $\{\mathbf{A}_i\}_i$ defined by $\{g(p_i)\}_i$ (Eq.(6)).

thus

$$\text{vol}(\mathbf{W}) = \int_{\mathbf{A}} \mathbf{F} \cdot \mathbf{n} \, d\mathbf{A}, \quad (5)$$

i.e., we can compute the volume of \mathbf{W} in terms of a flux through the boundary of \mathbf{W} .³ Now, without loss of generality, assume that \mathbf{V} is given by a simplicial polytope. The boundary of such a polytope is defined by a set of $(d-1)$ -simplices; for example, the boundary of a simplicial polytope in 2D is a set of 1-simplices (i.e., line segments). We can approximate the boundary \mathbf{A} by flowing the vertices of the $(d-1)$ -simplices defining the boundary of \mathbf{V} through g . Denoting the resulting set of simplices by $\{\mathbf{A}_i\}_i$, we have

$$\text{vol}(\mathbf{W}) \approx \sum_{\mathbf{A}_i} \mathbf{F}(\mathbf{A}_i^{(c)}) \cdot \mathbf{A}_i^{(n)}, \quad (6)$$

where \mathbf{A}_i is the i -th simplex, $\mathbf{A}_i^{(c)}$ its centroid, and $\mathbf{A}_i^{(n)}$ its outward-facing normal. The approximation error is rooted in the assumption that the true boundary patch in \mathbf{A} corresponding to a transformed simplex \mathbf{A}_i is linear. The larger the set of simplices approximating the boundary \mathbf{A} the better the estimate; see Fig. 2 for a summary of this section.

4.2. Stochastic Estimation in Target Space

One drawback of the method described in Eq.(6) is that it requires first constructing the set of simplices $\{\mathbf{A}_i\}_i$ in base space before we can apply the divergence theorem. In particular, we would need to recompute the centroids $\mathbf{A}_i^{(c)}$ and normals $\mathbf{A}_i^{(n)}$ every time $\{\mathbf{A}_i\}_i$ changes. Preferable is a direct integration over the boundary $\mathbf{S} := \partial\mathbf{V}$ in target space using an appropriate transformation of \mathbf{F} .

³We note that \mathbf{F} is not unique and other choices are possible.

Lemma 2. Let $d\mathbf{A}$ and $d\mathbf{S}$ be the area vectors in base space and target space, respectively. Then we have $\int_{\mathbf{A}} \mathbf{F} \cdot d\mathbf{A} = \int_{\mathbf{S}} \mathbf{G} \cdot d\mathbf{S}$, with $\mathbf{G} := |J|J^{-1}\mathbf{F}$ and $J := \nabla g$.

Proof. Consider a simplex with vertices p_i ($i = 1, 2, \dots, d$) in target space and its corresponding points $g(p_i)$ defining a simplex $\Delta\mathbf{A} \in \{\mathbf{A}_i\}_i$ in base space. g can be approximated with a Taylor expansion

$$g(\mathbf{x} + \epsilon) = g(\mathbf{x}) + J\epsilon + O(\|\epsilon\|_2^2), \quad (7)$$

where J is the Jacobian at the centroid of the simplex. With $\mathbf{F} = \mathbf{F}(\Delta\mathbf{A}^{(c)})$ denoting the field at the centroid, we can write out $\mathbf{F} \cdot \Delta\mathbf{A}^{(n)}$ as (see Appendix A for a discussion on computing surface normals)

$$\mathbf{F} \cdot \Delta\mathbf{A}^{(n)} = \frac{1}{(d-1)!} \begin{vmatrix} \mathbf{F} & J(p_2 - p_1) + 2O(\|\epsilon\|_2^2) \\ & J(p_3 - p_1) + 2O(\|\epsilon\|_2^2) \\ & \vdots \\ & J(p_d - p_1) + 2O(\|\epsilon\|_2^2) \end{vmatrix}. \quad (8)$$

In the limit $\Delta\mathbf{A} \rightarrow 0$, we have $\Delta\mathbf{A}^{(n)} \rightarrow d\mathbf{A}$ and $\|\epsilon\|_2^2 \rightarrow 0$:

$$\mathbf{F} \cdot d\mathbf{A} = \frac{1}{(d-1)!} J \begin{bmatrix} J^{-1}\mathbf{F} \\ p_2 - p_1 \\ p_3 - p_1 \\ \vdots \\ p_d - p_1 \end{bmatrix} = \mathbf{G} \cdot d\mathbf{S}, \quad (9)$$

where $\mathbf{G} = |J|J^{-1}\mathbf{F}$ \square

For notational convenience we assume $|J| > 0$ so that outward-facing surface normals in base space remain outward-facing in target space; the general case requires straightforward tracking of their signs. Interestingly, \mathbf{G} has a tractable divergence, paving the way for an application of the divergence theorem in target space.

Lemma 3. With \mathbf{G} defined as in Lemma 2, we have $\text{div}(\mathbf{G}) = |J|$.

Proof.

$$\begin{aligned} \nabla \cdot \mathbf{G} &= \nabla \cdot (\text{adj}(J)\mathbf{F}) \\ &= (\nabla \cdot \text{adj}(J))\mathbf{F} + \text{tr}(\text{adj}(J)\nabla_x\{\mathbf{F}\}) \\ &= d^{-1}\text{tr}(\text{adj}(J)J) + (\nabla \cdot \text{adj}(J))\mathbf{F} \\ &= |J| + (\nabla \cdot \text{adj}(J))\mathbf{F} \\ &= |J|, \end{aligned} \quad (10)$$

because $\text{tr}(\text{adj}(J)J) = d|J|$. Furthermore, (Evans, 2010) shows $\nabla \cdot \text{adj}(J) = 0$ for any C^2 -map \square

Lemma 3 allows us to close the loop and tie the field \mathbf{G} back to our original objective of computing $P(\mathbf{x} \in \mathbf{V})$. Indeed, an application of Eq.(4) and Eq.(1) shows

$$\int_{\mathbf{S}} \mathbf{G} \cdot d\mathbf{S} = \int_{\mathbf{V}} |J| d\mathbf{V} = \int_{\mathbf{V}} p(\mathbf{x}) d\mathbf{V} = P(\mathbf{x} \in \mathbf{V}). \quad (11)$$

See Fig. 3 for an overview of all equivalencies derived.

4.2.1. STOCHASTIC BOUNDARY FLUX ESTIMATOR

For a simplicial polytope \mathbf{V} with boundary \mathbf{S} given by non-overlapping simplices $\{\mathbf{S}_i\}_i$, we can leverage \mathbf{G} to define a *stochastic boundary flux (BF-S)* estimator of the cumulative density $P(\mathbf{x} \in \mathbf{V})$ using points sampled from the boundary:

$$\begin{aligned} \int_{\mathbf{S}} \mathbf{G} \cdot d\mathbf{S} &= \sum_i \int_{\mathbf{S}_i} \mathbf{G}(\mathbf{x}) \cdot \mathbf{S}_i^{(n)} d\mathbf{x} \\ &= \sum_i \mathbf{S}_i^{(A)} \int_{\mathbf{S}_i} \frac{\mathbf{G}(\mathbf{x})}{\mathbf{S}_i^{(A)}} \cdot \mathbf{S}_i^{(n)} d\mathbf{x} \\ &= \sum_i \mathbf{S}_i^{(A)} \int_{\mathbf{S}_i} \mathcal{U}_{\mathbf{S}_i}(\mathbf{x}) \cdot \mathbf{G}(\mathbf{x}) \cdot \mathbf{S}_i^{(n)} d\mathbf{x} \\ &= \sum_i \mathbf{S}_i^{(A)} \cdot \mathbb{E}_{\mathbf{x} \sim \mathcal{U}_{\mathbf{S}_i}} [\mathbf{G}(\mathbf{x}) \cdot \mathbf{S}_i^{(n)}], \end{aligned} \quad (12)$$

where \mathbf{S}_i is the i -th boundary simplex, $\mathbf{S}_i^{(A)}$ its area, and $\mathbf{S}_i^{(n)}$ its outward-facing unit normal. Alternatively, multiplying and dividing the surface integral $\int_{\mathbf{S}} \mathbf{G} \cdot d\mathbf{S}$ with the total surface area $(\sum_i \mathbf{S}_i^{(A)})$:

$$\int_{\mathbf{S}} \mathbf{G} \cdot d\mathbf{S} = \left(\sum_i \mathbf{S}_i^{(A)} \right) \cdot \mathbb{E}_{\mathbf{x} \sim \mathcal{U}_{\mathbf{S}}} [\mathbf{G}(\mathbf{x}) \cdot \mathbf{n}(\mathbf{x})], \quad (13)$$

where $\mathbf{n}(\mathbf{x})$ is the outward-facing unit normal at \mathbf{x} . Note that $\mathcal{U}_{\mathbf{S}}$ can be decomposed in terms of a categorical distribution $c_i = \mathbf{S}_i^{(A)} / \sum_j \mathbf{S}_j^{(A)}$ over the simplices \mathbf{S}_i and the uniform distributions $\mathcal{U}_{\mathbf{S}_i}$. More specifically, we have $\mathcal{U}_{\mathbf{S}}(\mathbf{x}) = \sum_i c_i \cdot \mathcal{U}_{\mathbf{S}_i}(\mathbf{x})$, wherein all but one of the terms are zero for a point \mathbf{x} on the surface \mathbf{S} — because the simplices are non-overlapping and the point \mathbf{x} belongs to exactly one of them.

4.3. Adaptive Estimation in Target Space

While the stochastic boundary flux estimator introduced in Section 4.2.1 is unbiased, it does not allow for a strategic placement of evaluation points in an iterative fashion. We can turn Eq.(12) into a sequential process by first approximating $\mathbb{E}_{\mathbf{x} \sim \mathcal{U}_{\mathbf{S}_i}} [\mathbf{G}(\mathbf{x}) \cdot \mathbf{S}_i^{(n)}]$ with a deterministic estimate and then performing prioritized iterative refinements.

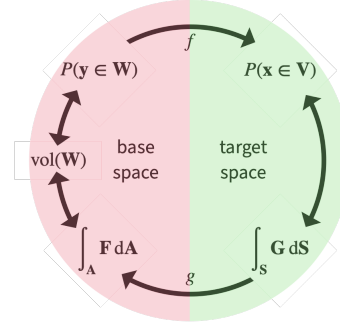


Figure 3. Equivalencies. We show equivalent expressions for the cumulative density of interest $P(\mathbf{x} \in \mathbf{V})$ and their associated spaces. The proposed estimator is motivated by a counter-clockwise chain of arguments, ultimately leveraging $\int_{\mathbf{S}} \mathbf{G} \cdot d\mathbf{S}$.

4.3.1. DETERMINISTIC BOUNDARY FLUX ESTIMATOR

Given a set of boundary simplices $\{\mathbf{S}_i\}_i$, we can approximate the expected dot-product in Eq.(12) by the average dot-product over the *vertices* of \mathbf{S}_i . Formally, this *adaptive boundary flux (BF-A)* estimator of $P(\mathbf{x} \in \mathbf{V})$ is given by

$$\int_{\mathbf{S}} \mathbf{G} \cdot d\mathbf{S} \approx \sum_i \mathbf{S}_i^{(A)} \cdot \overline{\mathbf{G}}(\mathbf{S}_i) \cdot \mathbf{S}_i^{(n)}, \quad (14)$$

where $\overline{\mathbf{G}}(\mathbf{S}_i)$ is the average \mathbf{G} -field over all vertices of \mathbf{S}_i . While Eq.(14) is a biased estimate of the cumulative density $P(\mathbf{x} \in \mathbf{V})$, its deterministic nature and inherent structure increase sample efficiency (e.g., prudent placement, reusable computations) and enable strategic refinements to arbitrary precision.

4.3.2. ITERATIVE REFINEMENT

The quality of the approximation in Eq.(14) can be controlled via iterative refinement of the initial set of boundary simplices $\{\mathbf{S}_i\}_i$. Each refinement step consists of a splitting operation that first introduces one new vertex at the midpoint of a boundary line segment⁴ and then splits all simplices sharing that edge. The key component of this splitting process is a priority queue Q managing the next boundary line segment l to split, where l is the longest edge of the simplex with highest priority according to a priority function Pr .

Pr is designed such that it gives high priority to simplices which *probably* have high error. As a general rule, the larger the simplex the larger the variation in the dot-products, and hence the larger the estimation bias. Although the area $\mathbf{S}_i^{(A)}$ of a simplex squarely fits the definition of size, it can be a misleading measure that should not be used in isolation — see Fig. 4 for an illustrated explanation. Therefore, we also use the total edge length as a measure of size. While this

⁴The $(d-1)$ -simplices $\{\mathbf{S}_i\}_i$ forming the boundary \mathbf{S} each consist of $\binom{d}{2}$ line segments.

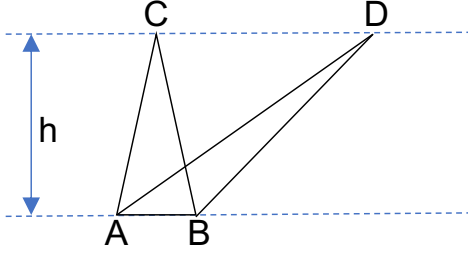


Figure 4. **Splitting Criterion (Total Edge Length).** For two simplices with equal area, the uncertainty about the dot-product within a simplex grows with a point’s distance to its closest vertex, motivating the use of total edge length as a splitting criterion.

approach works well in lower dimensions, we saw marked improvements in terms of sample efficiency in higher dimensions after complementing these two criteria with the standard deviation of the dot-products at the vertices. Taken together, we define the priority of the i -th simplex \mathbf{S}_i as

$$\Pr(\mathbf{S}_i) = \mathbf{S}_i^{(A)} \times (\sigma_d(\mathbf{S}_i) + \epsilon) \times \sum_{e_j \in \mathbf{S}_i} \|e_j\|_2^2, \quad (15)$$

where e_j is the j -th edge (1-simplex) constituting the simplex \mathbf{S}_i , $\sigma_d(\mathbf{S}_i)$ is the standard deviation of the dot-products – computed with the unit surface normal – across the simplex \mathbf{S}_i , and ϵ is a small number to guard against assigning a zero priority to large simplices whose dot-products at the vertices are all zero. See Appendix B for a summary of the entire splitting process in pseudo code.

4.4. Analysis

4.4.1. BEST CASE SCENARIOS

The integral of \mathbf{G} over a simplex \mathbf{S}_i can be computed exactly if the flow transformation g is: (a) linear over the simplex \mathbf{S}_i ; or (b) $\mathbf{G} \cdot \mathbf{S}_i^{(n)}$ is constant for all $\mathbf{x} \in \mathbf{S}_i$. The latter is equivalent to $\mathbf{F} \cdot d\mathbf{A}$ being constant, such as for hyperspheres. In both cases, we have $\overline{\mathbf{G}}(\mathbf{S}_i) = \mathbb{E}_{\mathbf{x} \sim \mathcal{U}_{\mathbf{S}_i}}[\mathbf{G}(\mathbf{x})]$. In practice, it is rarely possible to realize these best cases, however, if the dot-product is locally-linear over the simplex, our biased estimate is a good approximation to the exact integral.

4.4.2. RUNTIME COMPLEXITY & IMPLEMENTATION CONSIDERATIONS

For a given simplicial polytope, the algorithm first computes the surface normals for each of the boundary simplices, which requires computing d determinants of $(d-1) \times (d-1)$ matrices for each boundary simplex. The total complexity of this step is thus $\mathcal{O}(kd^4)$, where k is the number of boundary simplices. Note that the surface normals do not need to be recomputed upon splitting edges as they remain the same.

When computing \mathbf{G} , one has to first flow the input to the uniform distribution and then compute the Jacobian-vector product of the backward-pass; in order to avoid computing the Jacobian-vector product, we can first compute the vector-Jacobian product $\mathbf{S}_i^{(n)\top} J^{-1}$ of the backward-pass followed by a dot-product with $|J|\mathbf{F}$ to obtain $\mathbf{S}_i^{(n)\top} |J| J^{-1} \mathbf{F}$. This avoids an extra backward-pass in PyTorch, which does not support forward-mode auto-differentiation of Jacobian-vector-products. In fact, the derivative of $\mathbf{S}_i^{(n)\top} |J| J^{-1} \mathbf{F}$ with respect to $\mathbf{S}_i^{(n)\top}$ yields exactly \mathbf{G} .

5. Experiments

We will now evaluate the proposed adaptive boundary flux estimator (BF-A) against traditional sampling-based estimators such as the Monte-Carlo (MC) and Importance Sampling (IS) estimators. For the purpose of evaluation, we train normalizing flows on k -dimensional ($k \in [2, 5]$) data derived from 4 tabular datasets open sourced on the UCI Machine Learning Repository (Dua & Graff, 2017) and preprocessed as in (Papamakarios et al., 2017): Power, Gas, Hepmass, and Miniboone. We construct normalizing flows from the following three architecture families: Glow ((Kingma & Dhariwal, 2018)), Masked Autoregressive Flows ((Papamakarios et al., 2017)), and FFIJORD ((Grathwohl et al., 2019)). For every pair (dataset, k), we obtain 2 random k -dimensional slices of the dataset over which we train the normalizing flows. In addition, we also consider how the capacities of these models affect the performance: for the two discrete flows (Glow and MAFs), we vary the number of hidden dimensions in the coupling networks and the number of flow transforms stacked together; for FFIJORD, we instead vary the number of hidden dimensions in each layer of the MLP parameterizing the ODE. For constructing discrete flows, we choose 3, 5 or 7 flow layers and construct coupling layers with 16, 32 or 64 hidden units. While one Glow layer corresponds to a sequence of (ActNorm) – (Glow Coupling) – (Invertible 1×1) transformations, one MAF layer corresponds to a sequence of (ActNorm) – (MAF Coupling) transformations. For continuous flows, we parameterize the neural ODE with 2 hidden layers, each consisting of 16, 32 or 64 hidden units. In summary, we obtain a total of 168 flow models for every $k \in [2, 5]$ by training 21 flow models (9 each from the 2 discrete flow families and 3 from the continuous flows) on 2 slices derived from each of the 4 datasets. We include training details and the box-plots of training log-likelihoods in Appendix C.

Generating Simplicial Polytopes. The crucial component in ensuring a fair and unbiased evaluation of the estimators is in uniformly sampling simplicial polytopes \mathbf{V} in target space such that they are not biased towards any specific regions or cumulative densities. In order to actually

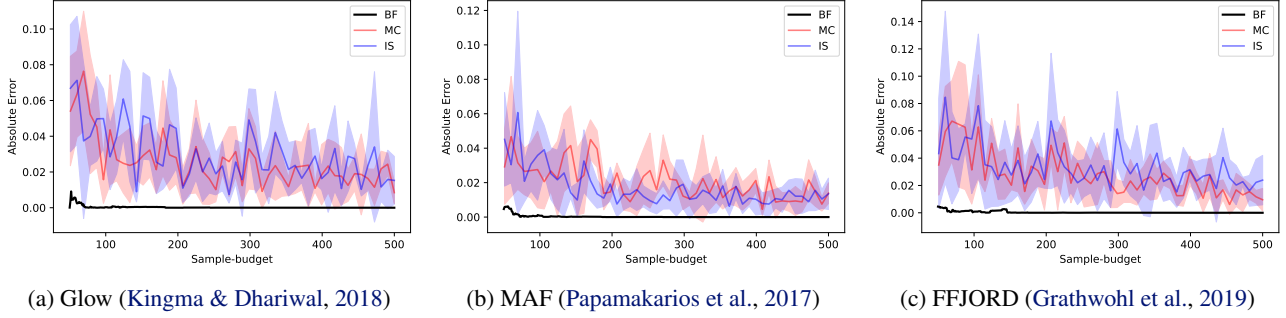


Figure 5. Sample Efficiency. We highlight the sample efficiency of the proposed adaptive boundary flux (BF-A) estimator as compared to Monte-Carlo (MC) and Importance Sampling (IS) estimators. We show absolute estimation errors for 3 flow architectures: two discrete normalizing flows (Glow and MAF) — composed of 7 flow-layers with 64 hidden units in their coupling nets — and one continuous normalizing flow (FFJORD) — parameterized by a 2-layer MLP with 64 hidden units in each layer. All models were trained on a 2D slice of the Power dataset, with volumes V given by convex hulls constructed from points sampled on the surface of spheres with radius 1.0, centered at points sampled from the flow.

sample a simplicial polytope, we construct a convex hull around a fixed number of points in target space. To ensure that convex hulls of varying sizes are equally explored, we sample these points from the boundary of a sphere centered at a flow sample and control the size of the convex hull by controlling the radius of the sphere. Convex hulls with a cumulative density of less than 0.01 are rejected. While the number of hull points affects the average size and cumulative density of the enclosed volume, it does not markedly change the average size of the simplices as defined in Section 4.3.2 and we therefore do not consider the number of hull points as an evaluation axis.

In our evaluation we consider 20 points to construct the hull, trading off lower cumulative densities against linear approximation of the spherical boundary; also note that all 20 points lie on the boundary of the hull and count against the sample budget of the BF-A algorithm. Furthermore, we consider spheres with radius 0.5, 0.75, or 1.0, amounting to a coverage radius of up to 1 standard deviation for our normalized data. Finally, in order to evaluate a normalizing flow model, we construct 5 convex hulls for each choice of the radius. Overall, we evaluate each CDF estimator over a total of 10,080 hulls.⁵

Evaluation. For each convex hulls we compute a reference cumulative density using $2M$ importance samples and evaluate all estimators against this gold standard based on their predicted cumulative density using a fixed sample budget K . Unlike our proposed adaptive boundary flux estimator (BF-A), which is deterministic, the Monte-Carlo (MC) and Importance Sampling (IS) estimators are stochastic; thus, in order to accurately capture the variance of these stochastic estimators, we collect results across 5 runs for

each hull. We then evaluate the estimators in terms of both relative and absolute errors. Table 1 shows the aggregate results across all 10,080 configurations with a sample budget of 4000 points. In the remainder of this section, we will unroll these results and analyze our estimator along individual evaluation axes.

Estimator	Absolute Error	Relative Error
IS	0.00572±0.01585	0.03000±0.04632
MC	0.00381±0.00381	0.04864±0.05178
BF-A (ours)	0.00152±0.00554	0.01822±0.06626

Table 1. Quantitative Evaluation (Aggregate): We show the absolute and relative errors of each estimator with a sample budget of 4000 points, averaged across all evaluation axes. The proposed BF-A algorithm outperforms the IS and MC estimators in terms of both the absolute and relative error.

Discussion. On average, our BF-A estimator obtains approximately $3.8\times$ and $2.5\times$ lower absolute errors than IS and MC, respectively, for a sample budget of $4k$ points (Table 1); likewise, we obtain $1.7\times$ and $2.7\times$ lower relative errors than IS and MC, respectively. For the specific case of 2D flows, we report relative errors that are better than IS by $11.6\times$ and MC by $22.1\times$ (Table 2); also see Fig. 5 for a qualitative comparison of the estimators for 2D flows in terms of the absolute deviation from the true cumulative density as obtained over a random hull: we note that in all 3 cases the proposed algorithm converges to the true estimate well within 500 samples while the stochastic estimates of the MC and IS estimators exhibit high variance. This pattern is consistent across our experiments with 2D flows and we find that our algorithm outperforms IS and MC by $30\times$ and $55\times$, respectively, for a sample budget of just 500 points. A comparison across different hull radii is shown in Table 3. We note that, while the absolute errors of all estimators

⁵10,080 hulls = $168 \frac{\text{models}}{\text{dim}} \cdot 4 \text{ dim} \cdot 5 \frac{\text{hulls}}{\text{models} \cdot \text{radii}} \cdot 3 \text{ radii}$

increase with increasing hull-sizes, the relative errors of MC decrease with increasing hull sizes, while those of IS and BF-A increase with increasing hull sizes; nonetheless, BF-A outperforms IS and MC in terms of both absolute and relative errors for the explored hull sizes. Additional quantitative evaluations can be found in the Appendix: in terms of different capacities (Appendix D; Tables 4-5), the observed trends are in line with the analysis above, both for discrete and continuous flows. We also note that varying the width of the coupling transform (in discrete flows) does not affect the observed trends as much as the depth of the flow transform. Finally, we observe similar trends across varying flow architectures as well (Appendix D; Table 6); also see Fig. 8 in Appendix D for a visual summary of all quantitative evaluations.

Our qualitative and quantitative evaluations show a marked improvement of the proposed method over traditional sampling-based estimators. BF-A benefits from our novel formulation of cumulative densities as boundary fluxes as well as from the sample efficiency enabled by the priority function Pr. Intuitively, the estimation error of the BF-A estimator can be traced back to how much the dot-product $\mathbf{G} \cdot \mathbf{n}$ can change for small changes in the input \mathbf{x} ; in fact, our motivation behind evaluating the estimators as a function of growing dimensions, growing hull-sizes, and growing model capacities is targeted towards testing how well our estimator can *adapt* to increasing complexity. We observe that while our method continues to outperform the sampling-based estimators with growing hull sizes (Table 3), model capacities (Appendix D; Table 4 and Table 5), varying flow architectures (Appendix D; Table 6), and data dimensions up to and including 4D, BF-A only performs comparably to the sampling-based estimators for a sample budget of $4k$ points with 5D flows (Table 2).

Limitations & Future Work. Future extensions of the proposed estimator could consider using higher-order information of the model, such as curvatures, in defining the priority function in order to improve the scalability of the method. Incorporating curvature information may also enable the definition of a more natural stopping criterion than sample budget. Another interesting extension to the adaptive estimator would be to split a *batch* of edges together as opposed to splitting a single edge at a time. Additionally, it remains to be explored how different choices of field \mathbf{F} can be useful in minimizing the estimation error for a given simplicial polytope. Finally, noting that our method works better with FFJORD than MAF and Glow on average (Appendix D; Table 6), even though they all obtain similar train log-likelihoods (Appendix C), one could also explore regularization methods that encourage smoother transformations between the target and base spaces.

Dims	Estimator	Absolute Error	Relative Error
2	IS	0.00737 \pm 0.01981	0.01620 \pm 0.02459
	MC	0.00482 \pm 0.00434	0.03101 \pm 0.03366
	BF-A (ours)	0.00071\pm0.00281	0.00146\pm0.00308
3	IS	0.00528 \pm 0.01564	0.02543 \pm 0.03618
	MC	0.00363 \pm 0.00381	0.05247 \pm 0.05202
	BF-A (ours)	0.00134\pm0.00584	0.00710\pm0.03254
4	IS	0.00405 \pm 0.00818	0.04495 \pm 0.05404
	MC	0.00274 \pm 0.00251	0.06576 \pm 0.06162
	BF-A (ours)	0.00237\pm0.00780	0.03209\pm0.08405
5	IS	0.00376 \pm 0.00640	0.07233\pm0.08153
	MC	0.00244\pm0.00218	0.07340 \pm 0.06483
	BF-A (ours)	0.00380 \pm 0.00658	0.07796 \pm 0.14184

Table 2. **Quantitative Evaluation (Dimension-wise):** We show the absolute and relative errors of each of the methods with a sample budget of 4000 points averaged across all the configurations separately for each dimensionality. We note that BF-A outperforms both IS and MC on average for 2D, 3D and 4D flows in terms of both absolute and relative errors.

Radius	Estimator	Absolute Error	Relative Error
0.5	IS	0.00338 \pm 0.01066	0.01895 \pm 0.02430
	MC	0.00336 \pm 0.00336	0.05670 \pm 0.05612
	BF-A (ours)	0.00073\pm0.00287	0.01016\pm0.04500
0.75	IS	0.00480 \pm 0.01327	0.02771 \pm 0.04061
	MC	0.00365 \pm 0.00350	0.04896 \pm 0.05205
	BF-A (ours)	0.00126\pm0.00460	0.01666\pm0.05429
1.0	IS	0.00808 \pm 0.01998	0.03941 \pm 0.05871
	MC	0.00425 \pm 0.00428	0.04292 \pm 0.04761
	BF-A (ours)	0.00229\pm0.00728	0.02500\pm0.08450

Table 3. **Quantitative Evaluation (Size-wise):** We show the absolute and relative errors of each of the methods with a sample budget of 4000 points averaged across all the configurations separately for each radius of the hull. On average, BF-A performs better than IS and MC in terms of both absolute and relative error.

Conclusion

Cumulative density functions are as fundamentally important as probability density functions, but cannot always be estimated efficiently and exactly. In this work, we propose a new stochastic CDF estimator derived as an adaptation of the divergence theorem by exploiting the diffeomorphic properties of flow that allow us to estimate CDF as the volume of the boundary. Furthermore, we demonstrate how this stochastic CDF estimator can be made more sample-efficient by reusing computations and strategically acquiring new points such that the estimate obtains a good CDF estimate with as few points as possible. In our evaluation of this new adaptive estimator, we find that it outperforms traditional sampling-based estimators in terms of sample-efficiencies and accuracies. We believe that our proposed efficient CDF estimator will help open up new application areas with Normalizing Flows.

Acknowledgements. This work was supported by a Borealis AI Graduate Fellowship. The authors also thank Vector Institute and Sageev Oore for supporting the project with computational resources.

References

- Abdar, M., Pourpanah, F., Hussain, S., Rezazadegan, D., Liu, L., Ghavamzadeh, M., Fieguth, P. W., Cao, X., Khosravi, A., Acharya, U. R., Makarevich, V., and Nahavandi, S. A review of uncertainty quantification in deep learning: Techniques, applications and challenges. *Inf. Fusion*, 2021.
- Armstrong, M. A. *Basic topology*. Springer Science & Business Media, 2013.
- Botev, Z. I. The normal law under linear restrictions: simulation and estimation via minimax tilting. *Journal of the Royal Statistical Society*, 2017.
- Botev, Z. I. and l’Ecuyer, P. Efficient probability estimation and simulation of the truncated multivariate student-t distribution. *Winter Simulation Conference (WSC)*, 2015.
- Chilinski, P. M. and Silva, R. Neural likelihoods via cumulative distribution functions. *Uncertainty in Artificial Intelligence, UAI*, 2020.
- Cundy, C. and Ermon, S. Flexible approximate inference via stratified normalizing flows. *Uncertainty in Artificial Intelligence, UAI*, 2020.
- Cunningham, J. P., Hennig, P., and Lacoste-Julien, S. Gaussian probabilities and expectation propagation. *Journal of Machine Learning Research*, 2013.
- Dai, B. and Seljak, U. Sliced iterative normalizing flows. *ICML Workshop on Invertible Neural Networks, Normalizing Flows, and Explicit Likelihood Models*, 2021.
- Dua, D. and Graff, C. UCI machine learning repository, 2017. URL <http://archive.ics.uci.edu/ml>.
- Evans, L. C. Partial differential equations. *Graduate studies in mathematics*, 2010.
- Genz, A. and Bretz, F. *Computation of multivariate normal and t probabilities*, volume 195. Springer Science & Business Media, 2009.
- Grathwohl, W., Chen, R. T. Q., Bettencourt, J., Sutskever, I., and Duvenaud, D. FFJORD: free-form continuous dynamics for scalable reversible generative models. *7th International Conference on Learning Representations, ICLR*, 2019.
- Kingma, D. P. and Dhariwal, P. Glow: Generative flow with invertible 1x1 convolutions. *Advances in Neural Information Processing Systems, NeurIPS*, 2018.
- Kobyzev, I., Prince, S., and Brubaker, M. Normalizing flows: An introduction and review of current methods. *IEEE Transactions on Pattern Analysis and Machine Intelligence*, 2020.
- Lange, K. Quadrature methods. *Numerical analysis for statisticians*, 1999.
- Liang, E., Yang, Z., Stoica, I., Abbeel, P., Duan, Y., and Chen, X. Variable skipping for autoregressive range density estimation. *International Conference on Machine Learning, ICML*, 2020.
- Liu, J. Z., Paisley, J. W., Kioumourtzoglou, M., and Coull, B. A. Accurate uncertainty estimation and decomposition in ensemble learning. *Advances in Neural Information Processing Systems, NeurIPS*, 2019.
- Mazaheri, B., Jain, S., and Bruck, J. Robust correction of sampling bias using cumulative distribution functions. *Advances in Neural Information Processing Systems, NeurIPS*, 2020.
- Mehta, A., Neukirchen, M., Pfetsch, S., and Poppensieker, T. Managing market risk: Today and tomorrow, 2012.
- Minka, T. P. Expectation propagation for approximate bayesian inference. *Uncertainty in Artificial Intelligence, UAI*, 2001.
- Papamakarios, G., Murray, I., and Pavlakou, T. Masked autoregressive flow for density estimation. *Advances in Neural Information Processing Systems, NeurIPS*, 2017.
- Papamakarios, G., Nalisnick, E., Rezende, D. J., Mohamed, S., and Lakshminarayanan, B. Normalizing flows for probabilistic modeling and inference. *Journal of Machine Learning Research*, 2021.
- Press, W. H., Teukolsky, S. A., Vetterling, W. T., and Flannery, B. P. *Numerical recipes in C*. Cambridge University Press, 1988.
- Richardson, M., Boudoukh, J., and Whitelaw, R. F. The best of both worlds: A hybrid approach to calculating value at risk, 1997.
- Ridgeway, K. and Mozer, M. C. Learning deep disentangled embeddings with the f-statistic loss. *Advances in Neural Information Processing Systems, NeurIPS*, 2018.
- Sun, W., Lee, C., and Lee, C. DFAC framework: Factorizing the value function via quantile mixture for multi-agent distributional q-learning. *International Conference on Machine Learning, ICML*, 2021.
- Wade, W. *An Introduction to Analysis*. Pearson, 2017.

A. Computing Surface Normals

In applying the divergence theorem, one would need to compute the surface normal vector. In the context of this paper, we compute surface normals to the $(d - 1)$ -dimensional simplices constituting the boundary: for example, we would need to compute the surface normal to line-segments in 2D, triangles in 3D, tetrahedrons in 4D and so on. By definition of $(d - 1)$ -dimensional simplices, they lie in a plane defined by $(d - 1)$ linearly independent vectors; since we are computing normals to $(d - 1)$ -dimensional simplices lying in \mathbb{R}^d , the vectors spanning the plane containing the simplex and the normal vector to this plane form a full basis of \mathbb{R}^d . In general, one could imagine solving a system of simultaneous equations in order to determine a vector normal to a given set of vectors. However, in this specific case, since we know that we are computing a normal vector to $(d - 1)$ linearly independent vectors, we can just define the normal vector to a simplex \mathbf{z} defined by the vertex set $\{z_i\}_i$ in terms of the determinant:

$$\mathbf{v} = \begin{vmatrix} \mathbf{e} \\ z_2 - z_1 \\ z_3 - z_1 \\ \vdots \\ z_d - z_1 \end{vmatrix} \quad (16)$$

where, \mathbf{e} is the orthonormal unit basis in \mathbb{R}^d . Since the determinant of a matrix containing two identical rows evaluates to 0, we can easily confirm that the dot product $\forall i \in [2, d], \mathbf{v} \cdot (z_i - z_1) = 0$. Also note that at a high level, this construction resembles the vector cross-product operation. In fact, similar to vector cross products, the vector norm of the \mathbf{v} is equal to the volume of the parallelotope spanned by the set of $(d - 1)$ linearly independent vectors $\{z_i - z_1\}_i$. Therefore, in order to derive the surface normal vector whose magnitude is equal to the volume of the simplex \mathbf{z} , we would need to divide \mathbf{v} with $(d - 1)!$:

$$\mathbf{z}^{(n)} = \frac{1}{(d - 1)!} \begin{vmatrix} \mathbf{e} \\ z_2 - z_1 \\ z_3 - z_1 \\ \vdots \\ z_d - z_1 \end{vmatrix} \quad (17)$$

Accordingly, for some vector \mathbf{w} , the dot-product $\mathbf{w} \cdot \mathbf{z}^{(n)}$ can be written as:

$$\mathbf{w} \cdot \mathbf{z}^{(n)} = \frac{1}{(d - 1)!} \begin{vmatrix} \mathbf{w} \\ z_2 - z_1 \\ z_3 - z_1 \\ \vdots \\ z_d - z_1 \end{vmatrix} \quad (18)$$

B. Pseudo-codes

Algorithm 1 Split edges and update the volume

Objects and Attributes:

edge: A 1 simplex object in \mathbb{R}^d having the following attributes:

- endPoints: the endPoints of the edge
- simplices: set of $d - 1$ -dimensional simplices that contains this edge

simplex: A $d - 1$ simplex object in \mathbb{R}^d having the following attributes:

- edges: the set of edges contained in the simplex
- unitSurfaceNormal: the unit surface normal of the simplex, adjusted so that it points outwards (or inwards) of the hull.
- volume: the volume of the simplex
- getVolumeElement: a method that will loop through the points and computes the mean dot-product.

Input:

edgeToSplit: The selected edge to split according to the priority function described in Eq.(15).

edges: Hashmap of Edges

- Allows $\mathcal{O}(1)$ retrieval of edge objects from the endpoints. If object does not exist in the queue, a new one is created and returned.

volume: The current estimated volume

Output:

newVolume

```

1: newVolume  $\leftarrow$  volume           ▷ Initialize the newVolume to be equal to the current volume
2: for simplex in edgeToSplit.simplices do
3:   simplex1  $\leftarrow$  new Simplex()
4:   simplex2  $\leftarrow$  new Simplex()
5:   simplex1.unitSurfaceNormal  $\leftarrow$  simplex.unitSurfaceNormal
6:   simplex2.unitSurfaceNormal  $\leftarrow$  simplex.unitSurfaceNormal
7:   simplex1.volume  $\leftarrow$  simplex.volume/2
8:   simplex2.volume  $\leftarrow$  simplex.volume/2
9:   for otherEdge in simplex.edges- $\{\text{edgeToSplit}\}$  do
10:    newEdge1  $\leftarrow$  edges.get(otherEdge.endPoint[0], edge.midPoint)
11:    newEdge2  $\leftarrow$  edges.get(otherEdge.endPoint[1], edge.midPoint)
12:    if otherEdge.hasEndPoint(edgeToSplit.endPoint[0]) then
13:      otherEdge.add(simplex1)
14:      simplex1.edges.add(otherEdge, newEdge1, newEdge2)
15:    else if otherEdge.hasEndPoint(edgeToSplit.endPoint[1]) then
16:      otherEdge.add(simplex2)
17:      simplex2.edges.add(otherEdge, newEdge1, newEdge2)
18:    else
19:      otherEdge.add(simplex1, simplex2)
20:      newEdge1.add(simplex1, simplex2)
21:      newEdge2.add(simplex1, simplex2)
22:      simplex1.edges.add(otherEdge, newEdge1, newEdge2)
23:      simplex2.edges.add(otherEdge, newEdge1, newEdge2)
24:      otherEdge.remove(simplex)
25:   newVolume  $\leftarrow$  newVolume - simplex.getVolumeElement()
26:   newVolume  $\leftarrow$  newVolume + simplex1.getVolumeElement()
27:   newVolume  $\leftarrow$  newVolume + simplex2.getVolumeElement()
28: return newVolume

```

Algorithm 2 getVolumeElement of Simplex Object

Objects and Attributes:

edge: A 1 simplex object in \mathbb{R}^d having the following attributes:

- endPoints: the endPoints of the edge
- simplices: set of $d - 1$ simplices that contains this edge

simplex: A $d - 1$ simplex object in \mathbb{R}^d having the following attributes:

- edges: the set of edges contained in the simplex
- unitSurfaceNormal: the unit surface normal of the simplex, adjusted so that it points outwards (or inwards) of the hull.
- volume: the volume of the simplex
- getVolumeElement: a method that will loop through the points and computes the mean dot-product.

Input:

simplex: A simplex object

flow: The normalizing flow

D: Number of dimensions

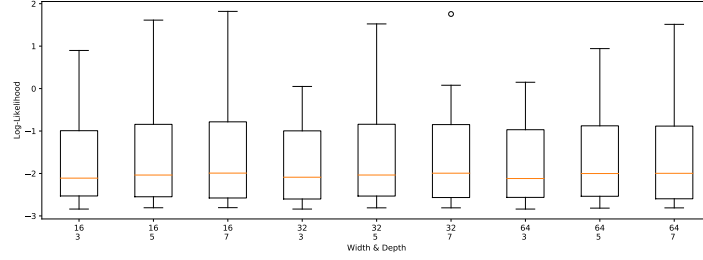
Output:

volume

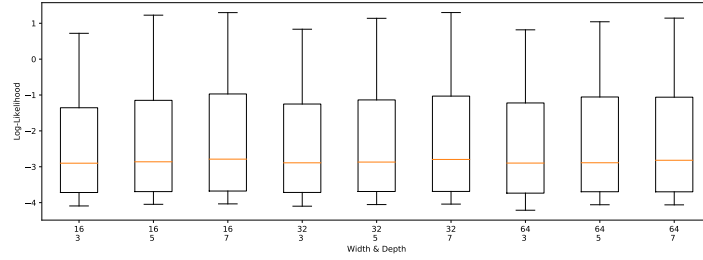
```
1: volumeElement  $\leftarrow$  0
2: for point in simplex.points() do
3:   volumeElement  $\leftarrow$  volumeElement + simplex.volume*flow.dotProduct(point, simplex.unitSurfaceNormal)
4: return volumeElement
```

C. Training Details and Log-likelihoods

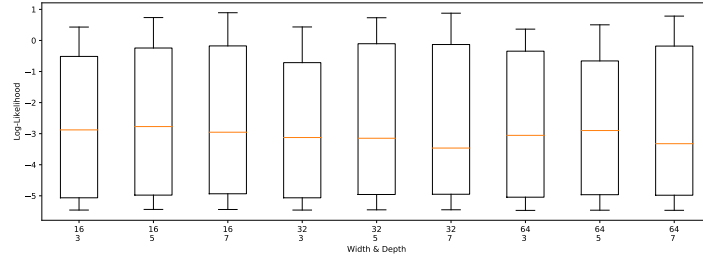
For all normalizing flows, we train the models with a batch size of 10k and stop when the log-likelihoods do not improve over 5 epochs. For the continuous flows, we used the exact divergence for computing the log-determinant. We used exp-scaling in the affine coupling layer of both MAF and Glow models – and, in order to prevent numerical overflows, we applied a tanh nonlinearity before the exp-scaling. Finally, we used softplus as our activation function for both the Neural ODE and coupling networks. From Fig. 6 and Fig. 7, we observe both the Continuous and Discrete flows obtain similar log-likelihoods and are able to fit the training data well.



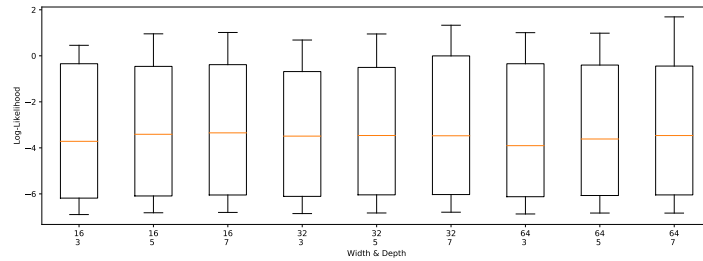
(a) 2D



(b) 3D

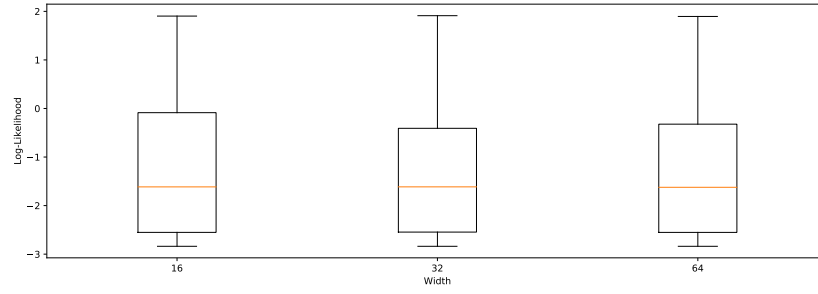


(c) 4D

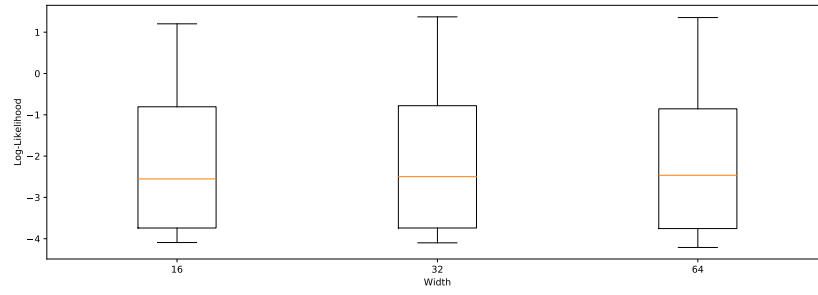


(d) 5D

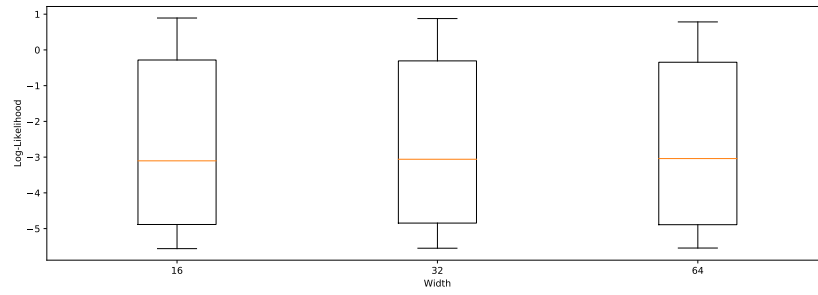
Figure 6. Log-Likelihoods (Discrete Flows).



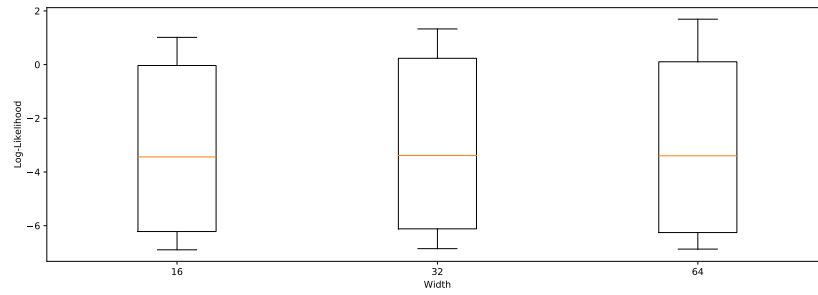
(a) 2D



(b) 3D



(c) 4D



(d) 5D

Figure 7. Log-Likelihoods (Continuous Flows).

D. Extended Results

In this section, we include results that evaluate our algorithm as a function of flow-architectures and their capacities. We also include plots to visually summarize our quantitative results.

Depth	Estimator	Absolute Error	Relative Error	Width	Estimator	Absolute Error	Relative Error
3	IS	0.00449±0.01048	0.02683±0.04063	16	IS	0.00552±0.01409	0.03095±0.04505
	MC	0.00359±0.00334	0.04844±0.05345		MC	0.00368±0.00335	0.04851±0.05277
	BF-A (ours)	0.00115±0.00479	0.01719±0.07362		BF-A (ours)	0.00195±0.00767	0.02290±0.07088
5	IS	0.00562±0.01381	0.03167±0.04787	32	IS	0.00544±0.01357	0.02940±0.04310
	MC	0.00372±0.00336	0.04833±0.05216		MC	0.00365±0.00334	0.04782±0.05253
	BF-A (ours)	0.00142±0.00536	0.02221±0.07773		BF-A (ours)	0.00130±0.00609	0.01944±0.07800
7	IS	0.00585±0.01499	0.03113±0.04583	64	IS	0.00501±0.01200	0.02932±0.04666
	MC	0.00375±0.00342	0.04776±0.05186		MC	0.00374±0.00342	0.04820±0.05217
	BF-A (ours)	0.00192±0.00775	0.02470±0.08521		BF-A (ours)	0.00125±0.00396	0.02184±0.08754

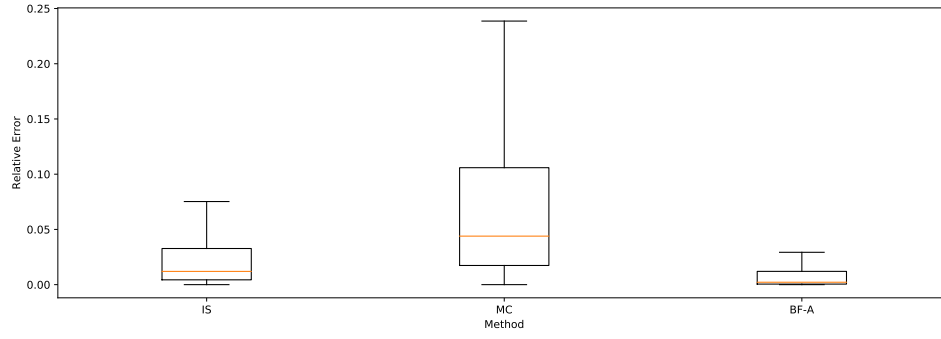
Table 4. **Quantitative Evaluation (Capacity - Glow and MAF)**: We show the absolute and relative errors of each of the methods with a sample budget of 4000 points as a function of the depth and width of discrete flows as explained; we see that BF-A outperforms both IS and MC.

Width	Estimator	Absolute Error	Relative Error
16	IS	0.00631±0.02026	0.02975±0.04846
	MC	0.00383±0.00472	0.04961±0.04996
	BF-A (ours)	0.00171±0.00504	0.01430±0.03244
32	IS	0.00614±0.01808	0.03005±0.04966
	MC	0.00400±0.00420	0.04991±0.05094
	BF-A (ours)	0.00131±0.00343	0.01034±0.02098
64	IS	0.00701±0.02152	0.03080±0.04856
	MC	0.00432±0.00470	0.04914±0.05012
	BF-A (ours)	0.00170±0.00391	0.01132±0.02083

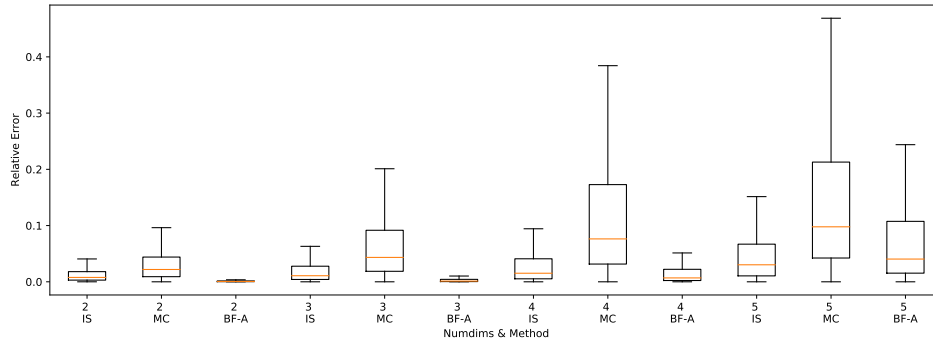
Table 5. **Quantitative Evaluation (Capacity - FFJORD)**: We show the absolute and relative errors of each of the methods with a sample budget of 4000 points as a function of the number of hidden units of two-layer MLPs parameterizing FFJORD as explained; we see that BF-A outperforms both IS and MC.

Flow	Method	Absolute Error	Relative Error
Glow	IS	0.00395±0.01131	0.02524±0.03818
	MC	0.00357±0.00328	0.05072±0.05421
	BF-A (ours)	0.00155±0.00726	0.01963±0.07250
MAF	IS	0.00667±0.01480	0.03445±0.05032
	MC	0.00379±0.00346	0.04568±0.05062
	BF-A (ours)	0.00145±0.00473	0.02311±0.08501
FFJORD	IS	0.00649±0.02000	0.03021±0.04890
	MC	0.00405±0.00455	0.04955±0.05034
	BF-A (ours)	0.00157±0.00417	0.01196±0.02529

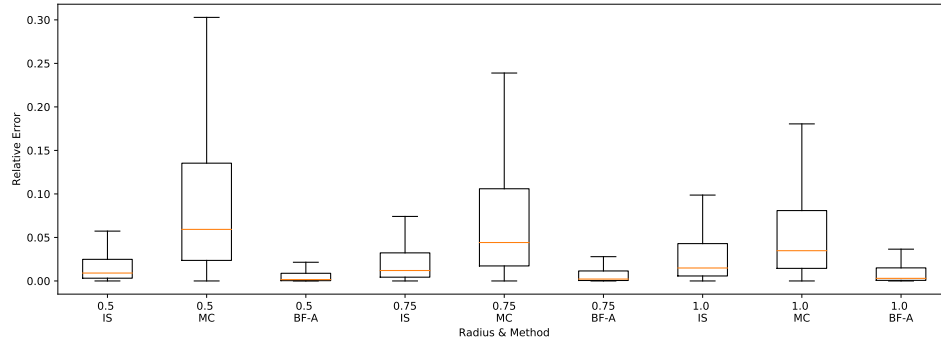
Table 6. **Quantitative Evaluation (Flow-Architecture)**: We show the absolute and relative errors of each of the methods with a sample budget of 4000 points as a function of the flow-architecture; we see that BF-A outperforms both IS and MC. Most interestingly, we find that our method is more efficient with Neural ODEs than with Glow or MAF – our analyses show that this can be attributed to the fact that Neural ODEs have much smoother diffeomorphic transformations than Glow and MAF. Perhaps more importantly, the Neural ODEs also obtain similar or better training log-likelihoods than Glow and MAF (Appendix C).



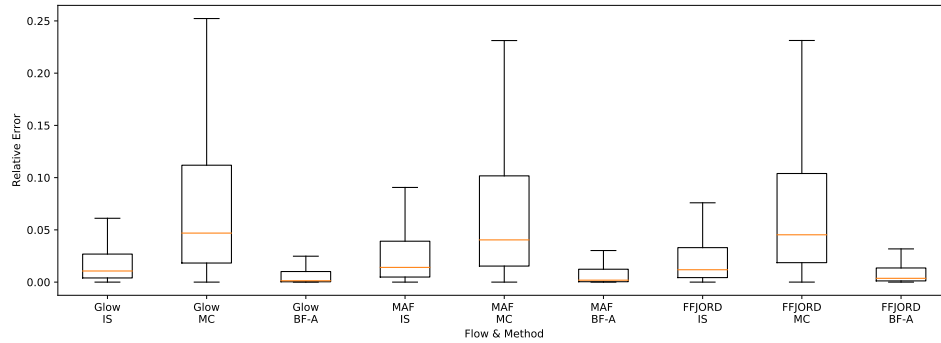
(a) Aggregate Evaluation of Estimators



(b) Evaluation of Estimators with Growing Dimensions



(c) Evaluation of Estimators with Growing Hull Sizes.



(d) Evaluation of Estimators as a function of Flow Architectures.

Figure 8. Visualizations of Quantitative Results.